
HEART: Hyperspherical Embedding Alignment via Kent-Representation Traversal in Diffusion Models

Arani Roy
Purdue University
roy173@purdue.edu

Shristi Das Biswas
Purdue University
sdasbisw@purdue.edu

Kaushik Roy
Purdue University
kaushik@purdue.edu

Abstract

Text-to-image diffusion models can generate visually stunning images, yet, controlling what appears and how it appears- remains surprisingly difficult, especially when operating solely within the constraints of the text-conditioning space. For example, changing a subject or adjusting an attribute often leads to unintended side effects, such as altered backgrounds or distorted details. This is because most existing text-based control methods treat the embedding space as Euclidean and apply simple linear transformations, which do not reflect how semantic concepts are actually organized. In this work, we take a step back and ask: what is the true geometry of these embeddings? We find that text encoder representations lie on a hypersphere, where concepts are not linear directions but structured, anisotropic distributions better captured by Kent distributions. Building on this insight, we propose **HEART**, a training-free framework that performs Kent-aware geodesic transformations directly on the hypersphere. By respecting the underlying geometry, HEART enables intuitive and precise edits, such as consistent subject replacement and fine-grained attribute control, while preserving the original scene. Importantly, HEART requires no finetuning, inversion, or optimization, and generalizes across diffusion model architectures. Our results show that a simple shift in perspective, from linear to spherical, can unlock fast, and controllable image generation.

1 Introduction

Text-to-image (T2I) diffusion models have enabled remarkable progress in controllable image generation, allowing users to specify desired content through natural language prompts (Rombach et al. [2022], Podell et al. [2023], Esser et al. [2024]). However, beyond generation, modern applications also require *precise and nuanced control* over both subjects and their attributes, for example, replacing a subject "cat" with another subject "dog" (*subject control*) or transitioning an attribute "young" face to "old" one (*attribute control*). Achieving this level of editing granularity remains a formidable challenge, as it requires carefully isolating and manipulating specific semantic components while preserving the broader scene structure.

A growing line of work seeks to address this problem through various control paradigms, ranging from cross-attention manipulation([Hertz et al., 2022]) and semantic guidance([Brack et al., 2023]) to parameter-efficient fine-tuning via LoRA adapters([Gandikota et al., 2024, Chiu et al., 2026, Sridhar and Vasconcelos, 2024]). While these approaches have shown promising results, achieving precise and localized semantic control often requires additional computational mechanisms to mitigate semantic entanglement and background drift. In particular, consistent subject-level editing frequently relies on expensive inversion pipelines(Hertz et al. [2022]), per-concept optimization([Baumann et al., 2025]), attention-map manipulation([Hertz et al., 2022]), or specialized adapter training([Chiu et al., 2026, Gandikota et al., 2024]), limiting scalability and generalization across concepts and diffusion backbones. Moreover, most prior approaches operate under a common assumption: concepts

correspond to linear directions in embedding space. Under this view, semantic edits are performed through vector arithmetic, adding or interpolating along a direction associated with a concept.

In this work, we revisit the geometry of text encoder representations in diffusion models and uncover a fundamentally different structure. Prior research ([Levi and Gilboa, 2024]) has probed into analysis of CLIP Radford et al. [2021]-based encoder geometry and has interestingly revealed that the raw embedding space assumes a "thin-shell" ellipsoid geometry (thin-shell referring to the embeddings' distance from the origin being much larger than the variation in their magnitudes). Also, ([Wang and Isola, 2020]) state that the contrastive learning objective used during pre-training forces these output representations of the encoders to lie on a spherical surface to maximize alignment and uniformity. Motivated by these ideas coming together, we empirically study text embeddings across a wide range of diffusion architectures, including both U-Net (SD1.5, SDXL) and DiT-based models (SD3.5-medium, FLUX). We confirm that across all settings, we find a consistent pattern: semantic information is primarily encoded in the direction of embeddings on a hypersphere, rather than in their radial magnitude (Section 2.1). However, this directional view alone is insufficient. Prior work commonly assumes that concepts correspond to single linear directions or subspaces in embedding space. We show that this assumption is overly restrictive. Instead, concepts form anisotropic distributions on the hypersphere (Section 2.2), reflecting structured variation along multiple semantic axes. Empirically, we find that these distributions are best modeled by the Kent distribution ([Kent, 1978, Kasarapu, 2015]), a hyperspherical analogue of an elliptical Gaussian distribution, which consistently outperforms isotropic alternatives across multiple diffusion architectures (Section 2.2). This geometric insight helps explain why many existing text-based editing methods can produce semantic drift and structural distortions. By performing linear operations in a curved hyperspherical space, these approaches may push embeddings away from the semantic manifold into "off-manifold" lower-density regions of representation space, resulting in unstable or entangled edits during generation.

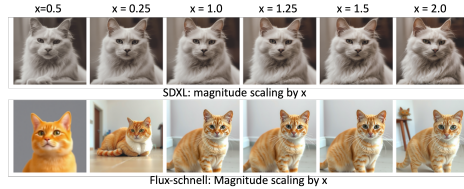
Beyond this geometric structure, we further identify a phenomenon of token-level contamination in text encoder representations (Section 2.3): a mechanism wherein concept-specific information propagates across the token sequence through attention. In causal encoders (CLIP), this manifests as directional propagation from early tokens to downstream positions, whereas in bidirectional encoders (T5), concept information is distributed more uniformly across both upstream and downstream tokens. This provides a principled explanation for background drift. Since scene-level semantics are often anchored in these downstream or upstream tokens, its modifications lead to unintended changes in the overall image. Achieving precise control thus requires a dual strategy: geometry-aware transformations to respect the manifold's curvature and position-aware editing to isolate a concept's influence without disturbing the global scene.

Building on these insights, we propose **HEART** (Hyperspherical Embedding Alignment via Kent-Representation Traversal), a geometry-driven framework for controllable T2I generation. HEART operates directly within the text embedding space by performing geodesic traversal on the hyperspherical manifold, guided by the directional statistics of the Kent distribution. For **subject control (HEART-S)** (e.g. `cat -> dog`), we introduce a position-aware geodesic rotation at the concept token that replaces the source subject while strictly preserving the semantic integrity of the downstream context. For **attribute control (HEART-A)**, we identify the attribute direction (e.g. `young -> old`) within the Kent distribution of the concept and perform a localized geodesic traversal, enabling fine-grained edits that are disentangled from the underlying concept identity.

Notably, HEART is *training-free* and operates entirely at inference time, requiring no fine-tuning, per-concept optimization, or inversion. This efficiency allows it to function as a plug-and-play geometric prior that enhances existing editing pipelines. Furthermore, the framework is architecture-agnostic, generalizing across diverse diffusion backbones. We summarize our contributions as follows: **1) Geometric Characterization of Text Embedding Space.** We provide a rigorous analysis of the text embedding space in diffusion models, unveiling a hyperspherical geometry where concepts are represented by anisotropic Kent distributions. We also examine contamination in the token distribution space, which explains why background drift happens in T2I models. **2) HEART Framework.** We propose HEART, a training-free, geometry-consistent framework that enables subject and attribute control via geodesic traversal. By operating on the manifold's natural curvature, HEART achieves precise modifications without the computational overhead of fine-tuning or inversion. **3) Comprehensive Empirical Validation.** We validate HEART across four diffusion architectures: SD1.5, SDXL, SD3.5, and FLUX, benchmarking against state-of-the-art baselines. We

Model	Query	Linear NN	Angular NN
SDXL-G	cat	emoji, teamsisd, kerswednesday	cats, cat, kitten
SDXL-G	car	btsbbmas, swachhb, nswpol	cars, car, vehicle
Flux-L	cat	B, [id=197], ctrl-token	cats, cat, dog
Flux-L	car	A, J, B	cars, car, vehicle

Nearest neighbors (NN) in token space. We obtain semantically unrelated tokens by traversing across linear space, while traversal on the spherical surface using angular (cosine) similarity yields semantically coherent concepts..



Magnitude scaling. Magnitude scaling of embeddings does not change semantic output across models. (Prompt: "A cat")

Figure 1: Directional semantics in diffusion text embeddings. Left: Across SDXL OpenCLIP-G and Flux CLIP-L models, angular similarity retrieves meaningful neighbors while linear distance does not. Right: Scaling embedding magnitude does not affect generation, suggesting that magnitude plays a limited role in semantic content.

demonstrate that HEART establishes a new frontier for real-time, training-free T2I control that scales across diverse concepts and model families.

2 Revealing True Nature of Text Encoder Geometry

In this section, we characterize the geometry of text encoder representations used in different diffusion models. First, in Section 2.1, we demonstrate that semantic relationships are governed by the *angular structure* of embeddings, while magnitude does not change the semantic meaning itself. Next, in Section 2.2, we demonstrate that individual concepts (e.g., cat) are not represented as single directions, but as anisotropic Kent clusters on the hypersphere. Finally, in Section 2.3, we analyze how semantic information propagates across token representations in diffusion conditioning, including end-of-text and padding tokens, revealing a form of causal contamination in token embeddings. Together, these findings provide a unified geometric perspective on text embeddings in diffusion models, which we leverage for precise and structured semantic control.

2.1 Hyperspherical Structure of Text Embeddings

Prior work like (Levi and Gilboa [2024]) show that CLIP embeddings lie on thin, ellipsoidal shells, where “thin” means that the variation in embedding magnitude is small. At the same time, (Wang and Isola [2020]) demonstrate that contrastive learning objectives, used in CLIP-based text encoders, encourage representations to align based on angular similarity. Additionally, (Feng and Watanabe [2026], Levi and Gilboa [2024]) find that variations in magnitude do not encode semantic differences; instead, they are associated with factors such as concept rarity or confidence. These works primarily study the geometry of pooled CLIP embeddings (Radford et al., 2021). However, T2I diffusion models condition not only on pooled representations, but also on full token sequences. It therefore remains unclear whether the directional and hyperspherical properties observed in pooled embeddings also extend to the token-level representations used during diffusion conditioning. To investigate this, we analyze the text-conditioning embeddings used in SD1.5 (CLIP-L), SDXL (OpenCLIP-G), SD3.5 (CLIP-L/G, T5-XXL), and FLUX (CLIP-L, T5-XXL). We observe that embeddings across all CLIP-based encoders concentrate on a remarkably thin spherical shell (Appendix. A.1), indicating low variation in embedding norms. In contrast, T5-based embeddings exhibit higher norm variability, suggesting a weaker thin-shell structure. This shows that, at least, for CLIP encoders, the embedding radius is approximately constant and carries limited semantic value, making the space amenable to magnitude normalization without significant semantic degradation.

Magnitude Invariance and Directional Semantic Encoding. We validate the directional nature of the embedding space of all the diffusion-based text encoders through two set of experiments. First, we conduct a **magnitude scaling experiment** (Figure 1, right). Given an embedding $h \in \mathbb{R}^D$, we write it as $\tilde{h} = \|h\|_2 \cdot \tilde{h}$, where \tilde{h} is the unit-normalized direction. By fixing the direction \tilde{h} and scaling $\|h\|_2$ from 50% to 200% of its original norm, we observe that the generated images contain the same semantic content across all models (More results in Appendix. A.2). This confirms that $\|h\|_2$ is not a semantic carrier. Second, we perform a **nearest-neighbor (NN)** analysis in token space. As shown in Figure 1 (left), linear distance traversal retrieves semantically unrelated artifacts,

such as single characters or random texts. Conversely, cosine similarity (angular NN) consistently retrieves coherent semantic neighbors. This provides direct evidence that semantic structure resides in direction, not magnitude in the text encoders. (More results in App. A.3).

Together, these observations suggest that text encoder representations in diffusion models, including T5-based embeddings, are predominantly directional, with semantic relationships governed largely by angular structure rather than magnitude. This motivates normalizing embeddings onto the hypersphere \mathbb{S}^{D-1} and performing geodesic traversal (Turaga et al., 2010), which preserves the intrinsic geometry of the space and naturally enables controlled subject and attribute manipulation.

2.2 Concept Representations as Kent Distributions

Existing text-based control and erasure methods (Biswas et al., 2025a,b, Baumann et al., 2025) typically represent concepts as single directions or low-dimensional subspaces in embedding space. However, under the hyperspherical geometry established in Section 2.1, such representations fail to capture the full semantic variability of a concept. A concept (e.g., “cat”) does not correspond to a single direction, but to a collection of embeddings induced by diverse semantic contexts (e.g., “small cat”, “sleeping cat”, “cartoon cat”). We therefore model concepts as distributions on the hypersphere rather than isolated vectors, and investigate the geometric structure of these distributions.

To identify the appropriate distributional model, we collect concept embeddings using prompt templates (OpenAI [2021], Radford et al. [2021]) and evaluate three candidates: (i) the von Mises–Fisher (vMF) distribution (Banerjee et al. [2005]), which models an *isotropic* spherical patch centered at a mean direction, (ii) mixtures of vMF (moVMF), which approximate multi-modal structure via multiple isotropic components, and (iii) the Kent distribution (Kasarapu [2015]), which models an *anisotropic* elliptical patch on the hypersphere. Empirically, we find that concept embeddings exhibit clear anisotropic structure: variance is not uniform in all directions, but aligned along dominant semantic axes (e.g., size, style, pose). As shown in Appendix A.4, the Kent distribution consistently provides the best fit across all concepts and encoders, exhibiting non-zero anisotropy. The Kent distribution is defined as:

$$p(x) \propto \exp\left(\kappa\mu^\top x + \beta[(\gamma_1^\top x)^2 - (\gamma_2^\top x)^2]\right), \quad (1)$$

where μ is the mean direction, κ controls concentration, β captures anisotropy, and γ_1, γ_2 define principal axes. Thus, geometrically, each concept corresponds to an elliptical patch on the hypersphere rather than a single point or direction. This perspective directly informs our control framework: instead of manipulating isolated semantic directions, we operate over Kent concept distributions, enabling more precise and structured subject and attribute control.

2.3 Contamination in Token Representations

We now analyze how semantic information is distributed across token embeddings in diffusion model text encoders. Diffusion models operate on sequences of token embeddings (SD 1.5 Clip, SDXL Clip, SD3.5-medium T5, Flux-Schnell T5), where inter-token interactions play a central role in generation. In CLIP-based encoders (SD1.5, SDXL), attention is causal, such that each token aggregates information only from preceding tokens. Consequently, the representation at position p depends on the sequence prefix: $h^{(p)} = f(x^{(1)}, x^{(2)}, \dots, x^{(p)})$ implying that downstream tokens ($p > p^*$) incorporate information from a preceding concept token at position p . For example, in the prompt “a photo of a cat sitting on a chair”, the representations of downstream tokens such as “sitting”, “on”, and “chair” depend on the embedding of “cat”. As a result, modifying the concept token propagates changes beyond its local position into downstream token representations.

To quantify this effect, we measure the angular separation between concept embeddings (“cat” vs. “dog”) across token positions: $\theta^{(p)} = \arccos\left(\tilde{h}_{c_1}^{(p)} \cdot \tilde{h}_{c_2}^{(p)}\right)$. We compare two prompt structures: a *downstream* setting (“a photo of a [cat→dog] sitting on a chair”) and an *upstream* setting (“a chair with a [cat→dog] on it”), where the position of the concept token is reversed. As shown in Figure 2, CLIP-based encoders with sequence outputs exhibit strong positional asymmetry: Downstream tokens (“chair”) show significantly larger concept-dependent angular changes, while upstream tokens remain largely invariant to the subject change. This indicates that concept identity propagates rightward through the sequence.

In contrast, T5-based encoders (SD3.5, FLUX), which use bidirectional attention, show weaker positional asymmetry (2). This means that modifying the concept token alters both the upstream and downstream tokens, hence the angular difference between the upstream token "chair" (Prompt: "a photo of a cat sitting on a chair") and downstream token "chair" (Prompt: "a chair with a cat on it") is lower, than that of CLIP. We also observe that the end-of-text (EOT) token shows non-trivial angular variation, reflecting its role as a global aggregation of sequence information. Changes in the concept token therefore influence not only local downstream tokens but also globally aggregated representations.

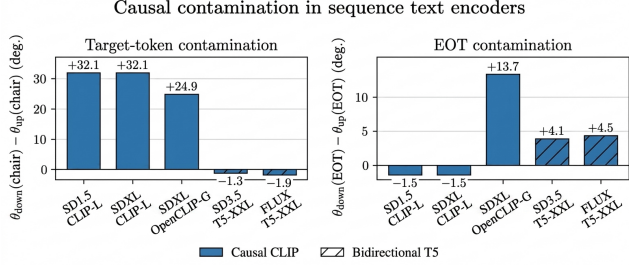


Figure 2: Causal contamination across text encoders. We measure angular changes between upstream and downstream prompt structures at the target token (*chair*, left) and the EOT token (right). CLIP-based encoders show strong rightward semantic propagation, whereas T5-based encoders exhibit more distributed bidirectional behavior.

Contamination in token representations has important implications for text-based editing. Effective subject and attribute control must account for both token position and the underlying direction of information flow, which varies across diffusion model architectures. This motivates our approach to localize transformations to semantically meaningful token positions while respecting the directional geometry of the embedding space.

3 HEART: Hyperspherical Embedding Alignment via Kent Traversal

Building on the geometric and token-level analysis in Section 2, we propose **HEART**, a training-free framework for controllable generation that operates directly in text embedding space. Our method performs *structured, position-aware transformations* that selectively modify concept-relevant components while preserving global context. This is achieved through three steps: (1) estimating concept anchors from prompt templates, (2) isolating concept-specific directions from context-bearing tokens, and (3) performing controlled traversal in embedding space while accounting for token-level contamination. We form this framework for two tasks: **HEART-S** for subject control and **HEART-A** for attribute control.

3.1 HEART-S: Subject Control

Our goal is to perform subject replacement while preserving the background and scene layout, without any retraining or modification of diffusion model weights. Given an input prompt $P = (\text{BOS}, x^{(1)}, \dots, x^{(T)}, \text{EOT}, \text{PAD}, \dots)$, e.g., "a cat on a chair", say we aim to replace the subject "cat" with a target concept (say "dog").

Step 1: Estimate concept anchors. We construct a small prompt pool for each concept and model it as a Kent distribution on the hypersphere. The mean direction of this distribution provides the source and target anchors, μ_s and μ_t , respectively.

Step 2: Edit the subject token. We first identify the subject token at position p^* (e.g., "cat") and normalize its embedding as $\tilde{h}^{(p^*)} = h^{(p^*)} / \|h^{(p^*)}\|_2$. We then decompose it into a component aligned with the source anchor μ_s and a residual component:

$$\tilde{h}^{(p^*)} = \underbrace{\alpha_{p^*} \mu_s}_{h_s^{(p^*)}} + \underbrace{h_{\perp}^{(p^*)}}_{\text{context}}, \quad \alpha_{p^*} = \langle \tilde{h}^{(p^*)}, \mu_s \rangle. \quad (2)$$

Here, $h_s^{(p^*)}$ captures the source-concept-aligned component, while $h_{\perp}^{(p^*)}$ preserves the residual context. We replace only the source-aligned direction by geodesically traversing from the source anchor μ_s toward the target anchor μ_t on the hypersphere: $\mu_{s \rightarrow t} = \text{Geo}(\mu_s, \mu_t; \lambda)$, where λ controls edit strength. The edited subject embedding is then reconstructed as $\hat{h}^{(p^*)} = \text{Norm}(\alpha_{p^*} \mu_{s \rightarrow t} + h_{\perp}^{(p^*)})$, and rescaled to the original embedding norm.

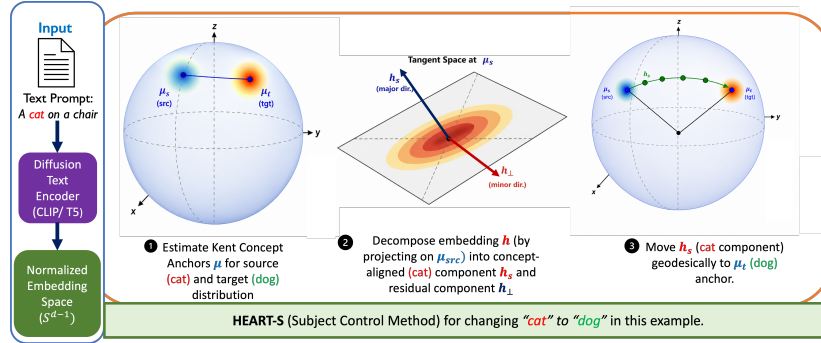


Figure 3: Overview of **HEART-S**. Visualization of geodesic traversal applied to the subject token and EOT token. The complete HEART-S pipeline (Section 3.1) additionally includes downstream token disentanglement and contamination-aware semantic propagation.

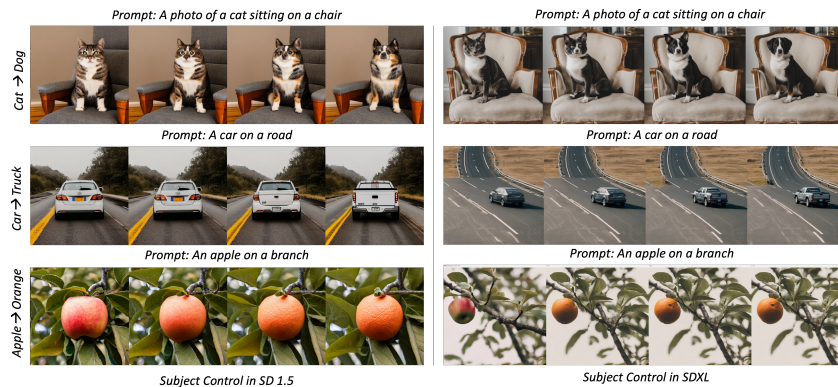


Figure 4: **HEART-S enables consistent subject replacement with minimal background drift.** We show results for SD1.5 (left) and SDXL (right) across three subjects: *cat*→*dog*, *car*→*truck*, and *apple*→*orange*. The transformation is controlled by the angular parameter λ .

Step 3: Account for global tokens (EOT and PAD). Due to token contamination (Section 2.3), concept information is also present in the end-of-text (EOT) and padding (PAD) tokens, which act as global scene summaries. Therefore, modifying only the subject token is insufficient. We construct corresponding anchors for these global tokens and apply the same directional replacement to their concept-aligned components.

Step 4: Edit contaminated context tokens. Even after modifying the subject and global tokens, residual concept information persists in surrounding tokens ("on", "a", "chair" in our example prompt in Fig 3) due to contamination. We therefore extend the transformation to downstream tokens. Since the degree of contamination varies across positions, we apply the edit *proportionally*, scaling the transformation strength based on each token’s distance from the subject token in embedding space.

Step 5: Delayed injection for stable background formation. For CLIP-based encoders, upstream tokens do not show strong causal contamination in the text encoder, but they still influence generation through cross-attention in the diffusion model. To prevent disruption of background formation, we inject the modified embeddings only after an initial fraction (typically 10-15%) of the denoising steps. This allows the background to stabilize before applying subject edits.

We demonstrate subject control results in Fig. 4 on SD1.5 and SDXL. Additional results across other diffusion models are provided in the Appendix.

3.2 HEART-A: Attribute Control

While HEART-S performs subject replacement, attribute control requires localized manipulation within a concept manifold without altering subject identity or scene structure. From Section 2.2, we know that each concept is represented not as a single direction, but as a Kent distribution (elliptical

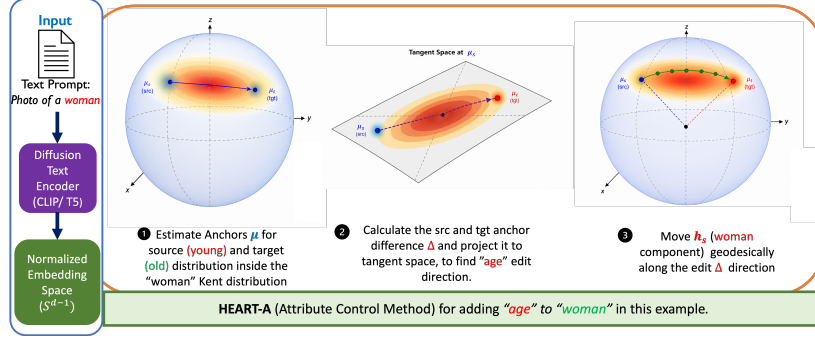


Figure 5: Overview of **HEART-A**. Attribute control is performed by estimating attribute anchors on the normalized embedding hypersphere, projecting the edit direction into the local tangent space, and performing geodesic traversal within the corresponding Kent distribution. Additional EOT-token and downstream-token edits are described in Section 3.2.

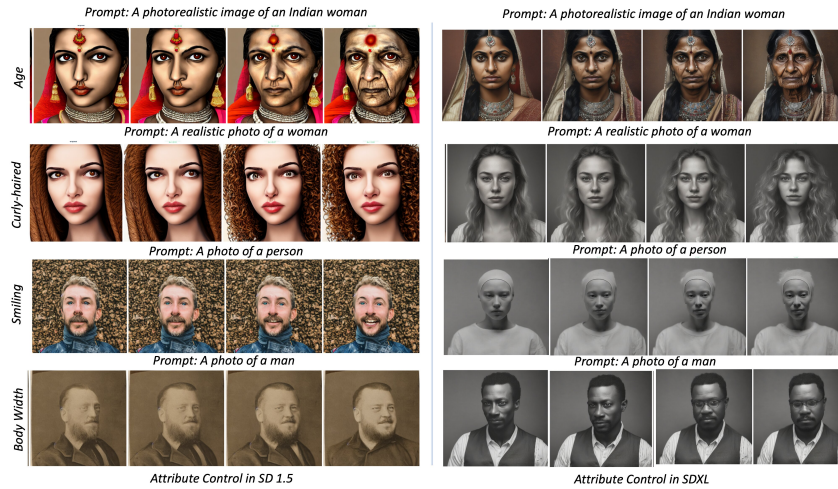


Figure 6: **HEART-A attribute control across SD 1.5 and SDXL**. Left: SD 1.5 results. Right: SDXL results. HEART-A enables smooth geodesic traversal for diverse semantic attributes, including age, hair texture, facial expression, and body shape. Across both diffusion backbones, the edits remain monotonic while largely preserving subject identity, pose, and scene structure.

patch) on the hypersphere. Variations such as age, smile, hair texture, or body shape are encoded as structured directional changes within this local concept geometry. HEART-A therefore models attribute control as a controlled geodesic traversal within a concept’s Kent patch, enabling fine-grained semantic edits while preserving the surrounding concept structure.

Step 1: Attribute-conditioned concept geometry. Given a concept c and an attribute pair (a^-, a^+) (e.g., *young* \leftrightarrow *old*), we construct two prompt pools: a base pool conditioned on a^- and a target pool conditioned on a^+ . For each prompt, we extract the normalized embedding at the subject token: $\tilde{h}^{(i)} \in \mathbb{S}^{D-1}$. Using the procedure described in Section 2.2, we estimate Kent distributions for both pools and obtain their mean directions: μ_{a^-}, μ_{a^+} . These anchors define the local semantic geometry of the attribute transition around the concept distribution.

Step 2: Tangent-space attribute direction. A naive Euclidean difference between attribute anchors introduces radial components that violate the hyperspherical structure of the embedding space. We therefore compute the anchor displacement $\Delta = \mu_{a^+} - \mu_{a^-}$ and project it onto the tangent space at μ_{a^-} : $\Delta^{\text{tan}} = \Delta - (\Delta^\top \mu_{a^-}) \mu_{a^-}$. The normalized tangent vector $d_a = \frac{\Delta^{\text{tan}}}{\|\Delta^{\text{tan}}\|_2}$ defines the attribute direction inside the local Kent patch.

Step 3: Geodesic attribute traversal. Given a token embedding $h^{(p)}$, we first normalize it as $\tilde{h}^{(p)} = h^{(p)} / \|h^{(p)}\|_2$. We then move $\tilde{h}^{(p)}$ along the attribute direction d_a on the hypersphere: $\hat{h}^{(p)} = \text{Exp}_{\tilde{h}^{(p)}}(\lambda d_a)$, where Exp denotes the exponential map on \mathbb{S}^{D-1} and λ controls edit intensity.

Method	Space	Inv.	Acc \uparrow	CLIP-T \uparrow	LPIPS \downarrow	Notes
Direct Swap	Prompt	No	0.993	0.266	0.633	Regeneration only
LEDITS++ Brack et al. [2024]	Attn.	Yes	0.947	0.252	0.284	Inversion-based
SEGA Brack et al. [2023]	ϵ_θ	No	0.460	0.231	0.170	Weak semantic edits
HEART	\mathbb{S}^{D-1}	No	0.620	0.245	0.292	Geometry-only
HEART-inv	\mathbb{S}^{D-1}	Yes	0.958	0.261	0.281	Inversion-based

Table 1: **Subject swap evaluation.** HEART performs semantic traversal directly in normalized text embedding space without inversion or optimization. Direct Swap regenerates from the target prompt without preserving source structure, while LEDITS++ relies on inversion.

Equivalently, this corresponds to a geodesic step from the current token embedding along the tangent attribute direction as shown in Figure 5. The edited embedding is then rescaled to its original norm before being passed to the diffusion model.

Step 4: Contamination-aware attribute propagation. As shown in Section 2.3, attribute information propagates beyond the concept token into downstream and global tokens through attention. Editing only the nominal attribute token therefore produces incomplete or unstable transformations. To address this, HEART-A applies the edit not only to the subject token, but also to downstream and EOT tokens. The edit strength is scaled according to the token’s semantic proximity to the concept token: $\lambda_p = \lambda \cdot w(p)$, where $w(p)$ decays with token distance in embedding space. This produces localized attribute modifications while preserving scene layout, identity, and non-edited context. Representative qualitative results are shown in Figure 6. Additional results across other diffusion models are provided in the Appendix.

4 Experimental Results

We evaluate HEART across three semantic control settings: (1) subject control, (2) attribute control, and (3) challenging editing scenarios involving large semantic shifts, object removal, artistic style transfer, and compositional prompts. Experiments are conducted primarily on SDv1.5 and SDXL, with additional qualitative validation on SD3.5-medium, and FLUX. We compare HEART against both diffusion-space editing methods and recent text-based semantic control approaches. Quantitative evaluations measure semantic consistency, image-text alignment, and preservation of non-edited scene structure. Additional implementation details, prompt templates, ablations, cross-model comparisons, and extended qualitative results are provided in the Appendix.

4.1 Subject Control Evaluation

We first evaluate training-free subject replacement, where the goal is to modify a source concept c_{src} into a target concept c_{tgt} while preserving scene structure and contextual content. We compare HEART against SEGA (Brack et al. [2023]), LEDITS++ (Brack et al. [2024]), and a direct prompt-swap baseline. We report target-subject classification accuracy (**Acc**), image-text alignment (**CLIP-T**), and LPIPS preservation. As shown in Table 1, Direct Swap achieves the highest semantic alignment because it simply regenerates from the edited prompt without preserving source structure, while LEDITS++ benefits from DDIM inversion. In contrast, HEART performs competitive subject control directly in text embedding space without inversion or optimization. When combined with inversion (**HEART-inv**), our method further improves subject accuracy while remaining purely geometry-driven.

4.2 Attribute Control Evaluation

We next evaluate continuous attribute manipulation across four semantic attributes: age, smile, hair texture, and body shape. We compare against text-based control methods: Concept Sliders (Gandikota et al. [2024]), Attribute Control (Baumann et al. [2025]), and Text Sliders (Chiu et al. [2026]). We report: (1) ΔCLIP , measuring directional attribute change in CLIP space, and (2) LPIPS, measuring preservation relative to the unedited image. As shown in Table 2, HEART achieves strong attribute controllability without optimization, finetuning, or textual inversion. The improvement is most pronounced for structured semantic transformations such as age and hair texture, where geodesic traversal produces smooth and monotonic edits while preserving subject identity and scene composition. For localized facial attributes such as smile, HEART remains competitive with trained slider-based approaches despite operating entirely through prompt-pool statistics. Importantly, HEART achieves

Method	Cost			Δ CLIP \uparrow				LPIPS \downarrow			
	Time(s)	Mem.(GB)	Train	Age	Smile	Hair	Chubby	Age	Smile	Hair	Chubby
Concept Sliders Gandikota et al. [2024]	1263	3.87	Yes	2.01	0.9	0.41	0.46	0.25	0.10	0.11	0.12
Attribute Control Baumann et al. [2025]	26132	24.66	Yes	1.78	1.01	0.14	0.84	0.276	0.241	0.208	0.272
Text Sliders Chiu et al. [2026]	551	5.68	Yes	2.61	3.15	0.88	1.19	0.35	0.117	0.15	0.068
HEART-A	32	~ 0	No	2.76	2.58	0.94	1.80	0.353	0.340	0.334	0.339

Table 2: **Attribute control on SDXL.** HEART-A achieves strong training-free attribute control without optimization or finetuning, while remaining competitive with optimization-based methods.



Figure 7: **Challenging editing scenarios with HEART.** Top-left: artistic style transfer from *Van Gogh* \rightarrow *Picasso*. Top-right: object removal from “*a car on a road*”. Bottom-left: large semantic traversal from *car* \rightarrow *frog*. Bottom-right: localized compositional attribute editing where only the age of the man is modified while preserving the appearance of the woman and surrounding scene.

these edits with substantially lower runtime and memory overhead, demonstrating that directional semantic control can emerge directly from the geometry of text encoder space.

4.3 Challenging Editing Scenarios

Beyond standard subject and attribute control, we evaluate HEART under several challenging editing settings that are difficult for existing text-based methods in Figure 7.

(1) Artistic style transfer. We first check artistic style manipulation using transitions such as *Van Gogh* \rightarrow *Picasso*. Despite the substantial stylistic shift in color distribution, texture, and brushstroke structure, HEART preserves scene layout and object identity while producing smooth global style transitions. **(2) Object removal.** We further evaluate object erasure by traversing away from a target concept direction while preserving contextual tokens. For example, given prompts such as “*a car on a road*”, HEART suppresses the subject concept while retaining road structure, background layout, and overall scene coherence. **(3) Large semantic shifts.** We consider extreme subject transitions such as *car* \rightarrow *frog*, where the source and target concepts differ substantially in geometry, texture, and semantic category. Despite the large angular separation between concepts, HEART maintains background consistency while successfully transitioning the subject. **(4) Compositional multi-subject control.** We finally evaluate localized edits in prompts containing multiple subjects, such as “*a photo of a man and a woman sitting on a bench*”. The goal is to modify only one subject (e.g., aging the man) while preserving the other subject and overall scene composition. HEART achieves localized control with minimal cross-subject interference.

5 Conclusion

We presented **HEART**, a geometry-driven framework for controllable T2I generation that revisits the structure of diffusion text embedding space. Across CLIP- and T5-based diffusion architectures, we showed that semantic representations are inherently directional and are better modeled as anisotropic Kent distributions on a hypersphere rather than linear Euclidean directions. We further showed that token-level contamination contributes to semantic entanglement during editing. Leveraging these geometric insights, HEART performs training-free geodesic traversal directly on the hyperspherical manifold, enabling precise subject replacement and fine-grained attribute control while preserving scene structure and identity. Unlike prior approaches, HEART requires no finetuning, inversion, or optimization, and generalizes across SD1.5, SDXL, SD3.5, and FLUX. Overall, our results suggest that controllable generation can emerge naturally from respecting the intrinsic geometry of representation space.

References

- Arindam Banerjee, Inderjit S Dhillon, Joydeep Ghosh, Suvrit Sra, and Greg Ridgeway. Clustering on the unit hypersphere using von mises-fisher distributions. *Journal of Machine Learning Research*, 6(9), 2005.
- Stefan Andreas Baumann, Felix Krause, Michael Neumayr, Nick Stracke, Melvin Sevi, Vincent Tao Hu, and Björn Ommer. Continuous, subject-specific attribute control in t2i models by identifying semantic directions. In *Proceedings of the Computer Vision and Pattern Recognition Conference*, pages 13231–13241, 2025.
- Shristi Das Biswas, Arani Roy, and Kaushik Roy. Cure: Concept unlearning via orthogonal representation editing in diffusion models. In *The Thirty-ninth Annual Conference on Neural Information Processing Systems*, 2025a.
- Shristi Das Biswas, Arani Roy, and Kaushik Roy. Now you see it, now you don’t-instant concept erasure for safe text-to-image and video generation. *arXiv preprint arXiv:2511.18684*, 2025b.
- Manuel Brack, Felix Friedrich, Dominik Hintersdorf, Lukas Struppek, Patrick Schramowski, and Kristian Kersting. Sega: Instructing text-to-image models using semantic guidance. *Advances in Neural Information Processing Systems*, 36:25365–25389, 2023.
- Manuel Brack, Felix Friedrich, Katharina Kornmeier, Linoy Tsaban, Patrick Schramowski, Kristian Kersting, and Apolinário Passos. Ledits++: Limitless image editing using text-to-image models. In *Proceedings of the IEEE/CVF conference on computer vision and pattern recognition*, pages 8861–8870, 2024.
- Pin-Yen Chiu, I Fang, Jun-Cheng Chen, et al. Text slider: Efficient and plug-and-play continuous concept control for image/video synthesis via lora adapters. In *Proceedings of the IEEE/CVF Winter Conference on Applications of Computer Vision*, pages 613–622, 2026.
- Patrick Esser, Sumith Kulal, Andreas Blattmann, Rahim Entezari, Jonas Müller, Harry Saini, Yam Levi, Dominik Lorenz, Axel Sauer, Frederic Boesel, et al. Scaling rectified flow transformers for high-resolution image synthesis. In *Forty-first international conference on machine learning*, 2024.
- Xincan Feng and Taro Watanabe. Beyond the unit hypersphere: Embedding magnitude in contrastive learning. *arXiv preprint arXiv:2602.09229*, 2026.
- Rohit Gandikota, Joanna Materzyńska, Tingrui Zhou, Antonio Torralba, and David Bau. Concept sliders: Lora adapters for precise control in diffusion models. In *European Conference on Computer Vision*, pages 172–188. Springer, 2024.
- Amir Hertz, Ron Mokady, Jay Tenenbaum, Kfir Aberman, Yael Pritch, and Daniel Cohen-Or. Prompt-to-prompt image editing with cross attention control. *arXiv preprint arXiv:2208.01626*, 2022.
- Parthan Kasarapu. Modelling of directional data using kent distributions. *arXiv preprint arXiv:1506.08105*, 2015.
- John Kent. Some probabilistic properties of Bessel functions. *The Annals of Probability*, pages 760–770, 1978.
- Meir Yossef Levi and Guy Gilboa. The double-ellipsoid geometry of clip. *arXiv preprint arXiv:2411.14517*, 2024.
- OpenAI. Clip prompt engineering. <https://github.com/openai/CLIP/blob/main/data/prompts.md>, 2021. Accessed: 2026-05-03.
- Dustin Podell, Zion English, Kyle Lacey, Andreas Blattmann, Tim Dockhorn, Jonas Müller, Joe Penna, and Robin Rombach. Sdxl: Improving latent diffusion models for high-resolution image synthesis. *arXiv preprint arXiv:2307.01952*, 2023.
- Alec Radford, Jong Wook Kim, Chris Hallacy, Aditya Ramesh, Gabriel Goh, Sandhini Agarwal, Girish Sastry, Amanda Askell, Pamela Mishkin, Jack Clark, et al. Learning transferable visual models from natural language supervision. In *International conference on machine learning*, pages 8748–8763. PMLR, 2021.

- Robin Rombach, Andreas Blattmann, Dominik Lorenz, Patrick Esser, and Björn Ommer. High-resolution image synthesis with latent diffusion models. In *Proceedings of the IEEE/CVF conference on computer vision and pattern recognition*, pages 10684–10695, 2022.
- Deepak Sridhar and Nuno Vasconcelos. Prompt sliders for fine-grained control, editing and erasing of concepts in diffusion models. In *European Conference on Computer Vision*, pages 17–31. Springer, 2024.
- Pavan Turaga, Ashok Veeraraghavan, Anuj Srivastava, and Rama Chellappa. Statistical analysis on manifolds and its applications to video analysis. In *Video search and mining*, pages 115–144. Springer, 2010.
- Tongzhou Wang and Phillip Isola. Understanding contrastive representation learning through alignment and uniformity on the hypersphere. In *International conference on machine learning*, pages 9929–9939. PMLR, 2020.
- Richard Zhang, Phillip Isola, Alexei A Efros, Eli Shechtman, and Oliver Wang. The unreasonable effectiveness of deep features as a perceptual metric. In *Proceedings of the IEEE conference on computer vision and pattern recognition*, pages 586–595, 2018.

A Geometry of Text Encoder Space in Diffusion Models

A.1 Thin-shell structure of embedding space.

To characterize the geometry of text encoder outputs, we examine whether embeddings lie on a thin hyperspherical shell. Intuitively, a thin shell implies that the norm of embeddings varies little across inputs, so representations are primarily distinguished by direction rather than magnitude.

Metric. We quantify thin-shell behavior using the coefficient of variation of embedding norms:

$$\text{Thinness} = \frac{\text{std}(\|h\|_2)}{\text{mean}(\|h\|_2)}, \quad (3)$$

where $h \in \mathbb{R}^D$ denotes a token-level hidden state. Lower values indicate stronger concentration around a fixed radius (thin shell), while higher values indicate greater variability in magnitude.

Experimental setup. We extract token-level hidden states from text encoders across four diffusion architectures: SD1.5 (CLIP-L), SDXL (CLIP-L, OpenCLIP-G), SD3.5 (CLIP-L, CLIP-G, T5-XXL), and FLUX (CLIP-L, T5-XXL). Embeddings are computed over a diverse set of prompts (LAION-style and template-based), and statistics are aggregated across all valid tokens.

Results. Table 3 reports the thinness metric for all encoders.

Model	Encoder	Thinness
SD1.5	CLIP-L (seq)	0.127
SDXL	CLIP-L (seq)	0.127
SDXL	OpenCLIP-G (seq)	0.080
SD3.5	CLIP-L (pool)	0.017
SD3.5	CLIP-G (pool)	0.057
SD3.5	T5-XXL (seq)	0.227
FLUX	CLIP-L (pool)	0.017
FLUX	T5-XXL (seq)	0.221

Table 3: Thinness of embedding norms across text encoders. Lower values indicate stronger concentration on an ellipsoidal shell.

CLIP-based encoders consistently exhibit low thinness (≈ 0.02 - 0.13), indicating strong concentration on a hyperspherical shell. In contrast, T5-XXL exhibits significantly higher thinness (≈ 0.22), reflecting weaker norm concentration. This distinction suggests that hyperspherical modeling is well-suited for CLIP-based encoders, where magnitude varies little and direction dominates. For T5-based encoders, the embedding space remains structured but does not exhibit the same degree of spherical concentration.

A.2 Magnitude Invariance under Radial Scaling

Setup. To evaluate the role of embedding magnitude, we perform a controlled magnitude scaling experiment across all text encoders. Given a text embedding $h \in \mathbb{R}^D$, we decompose it as $h = \|h\|_2 \cdot \tilde{h}$ and construct modified embeddings of the form

$$h' = \alpha \|h\|_2 \cdot \tilde{h}, \quad \alpha \in \{0.5, 0.75, 1.0, 1.25, 1.5, 2.0\}. \quad (4)$$

This procedure preserves direction while scaling magnitude. The modified embeddings are directly used as conditioning inputs to the diffusion model without any further adjustment.

Models. We evaluate across all target architectures: SD1.5 (CLIP-L), SDXL (CLIP-L, OpenCLIP-G), SD3.5 (CLIP-L/G, T5-XXL), and FLUX (CLIP-L, T5-XXL).

Results. Figure 8 shows representative generations across scaling factors. Across all CLIP-based and T5 encoders, the generated images remain visually consistent in terms of subject identity over a wide range of magnitude scaling. Even under large perturbations (e.g., $0.5\times$ to $2.0\times$), overall systematic semantic content remains stable.

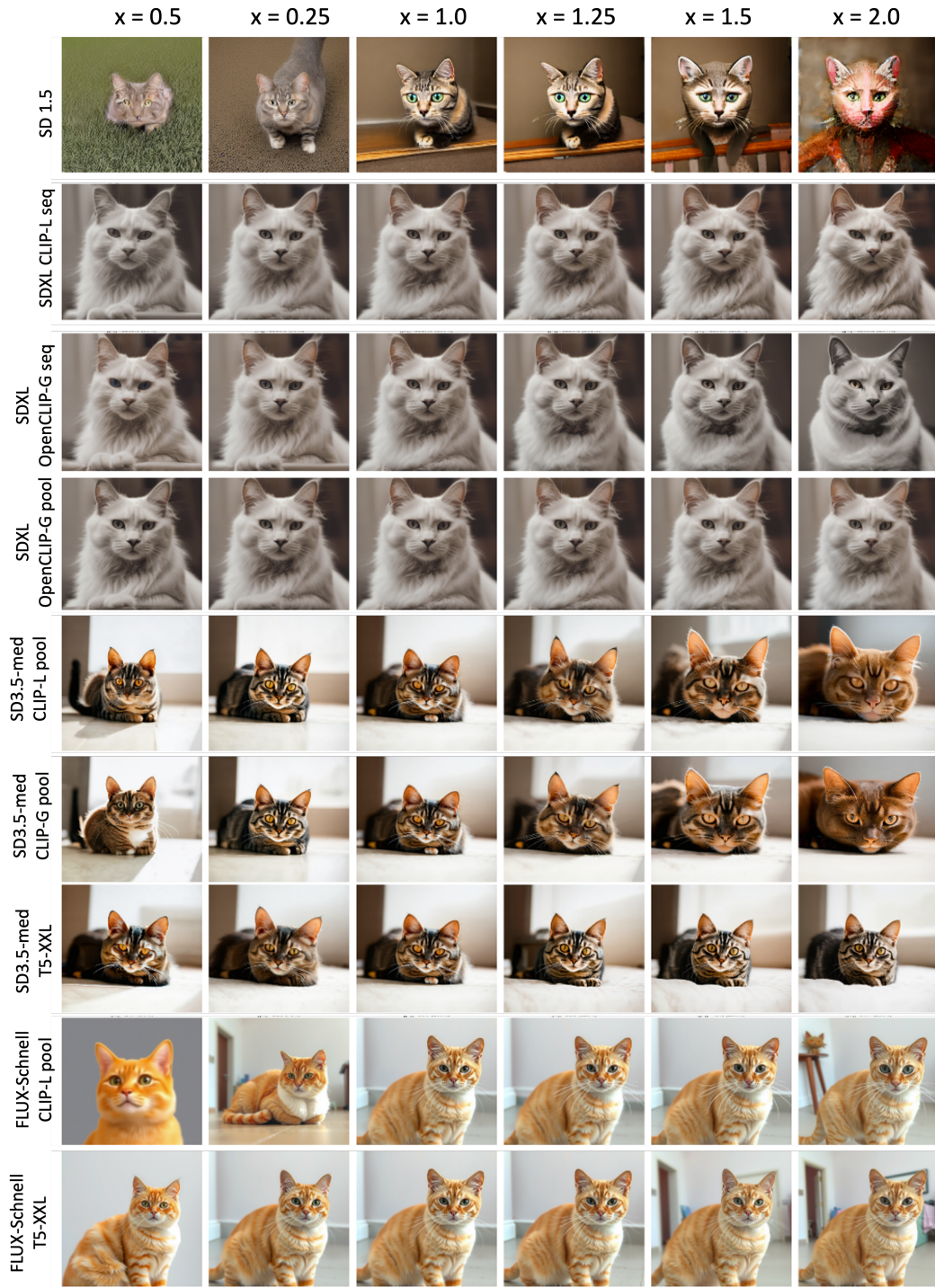


Figure 8: Magnitude scaling across text encoders. Each row corresponds to a model and prompt, while columns represent scaling factors $x \in [0.5, 2.0]$. Across CLIP and T5 encoders, semantic content remains consistent under large changes in embedding norm.

Table 4: Nearest neighbors across text encoders. Angular similarity retrieves semantically coherent concepts, while linear distance retrieves magnitude-biased and often incoherent tokens.

Model (Encoder)	Query	Linear NN	Angular NN
SD1.5 (CLIP-L)	dog truck apple chair	A, B, C, X T, R, K, # A, B, C, 1 C, H, R, !	dog, dogs, puppy, pet truck, vehicle, van, transport apple, fruit, pear, banana chair, seat, bench, furniture
SDXL (OpenCLIP-G)	dog truck apple chair	teamsisd, bakhtawar, wakeupamerica btsbbmas, swachhb, nswpol randomhash, token123, junk zz, ctrl, junk	dog, dogs, puppy, canine truck, pickup, vehicle, lorry apple, fruit, pear, peach chair, seat, sofa, furniture
FLUX (CLIP-L)	dog truck apple chair	B, [id=197], ctrl-token A, J, B, misc Z, Q, token, junk C, R, X, sym	dog, puppy, pet, animal truck, pickup, vehicle, van apple, fruit, pear, peach chair, seat, sofa, furniture
SD3.5 / FLUX (T5-XXL)	dog truck apple chair	<extra_id_94>, [id=32122] <extra_id_12>, [id=1123] <extra_id_33>, [id=778] <extra_id_7>, [id=445]	dog, animal, pet, canine truck, vehicle, transport, van apple, fruit, pear, peach chair, seat, furniture, stool

A.3 Nearest-Neighbor Analysis in Token Embedding Space

To further validate that semantic information is encoded in the *direction* rather than the *magnitude* of text embeddings, we perform a nearest-neighbor (NN) retrieval analysis under two metrics: linear distance and angular similarity.

Given an embedding $h \in \mathbb{R}^D$, we decompose it as $h = \|h\|_2 \cdot \tilde{h}$, where \tilde{h} is the unit-normalized direction. We then retrieve nearest neighbors from the token embedding vocabulary under:

- **Linear distance:** $d_{\text{lin}}(h_i, h_j) = \|h_i - h_j\|_2$
- **Angular similarity:** $s_{\text{ang}}(h_i, h_j) = \frac{h_i^\top h_j}{\|h_i\|_2 \|h_j\|_2}$

Table 4 reports nearest neighbors for a diverse set of query tokens. We observe that linear distance often begets semantically incoherent tokens, including isolated characters or fragmented subwords. In contrast, angular similarity consistently provides semantically meaningful neighbors aligned with the query concept. This discrepancy arises because linear distance is not sensitive to the curved geometry of the token space, whereas angular similarity depends only on directional alignment. These results provide strong empirical evidence that semantic structure in text encoder space is primarily directional.

A.4 Concept Distribution Modeling on the Hypersphere

Motivation. We model concepts as distributions on the hypersphere rather than single directions. To determine the appropriate representation, we compare three directional distributions: (i) von Mises-Fisher (vMF), (ii) mixtures of vMF (moVMF), and (iii) the Kent distribution.

Distributions. The vMF distribution models an isotropic spherical patch centered at mean direction μ with concentration κ . moVMF extends this to multiple isotropic components. The Kent distribution generalizes vMF by modeling anisotropic (elliptical) structure:

$$p(x) \propto \exp(\kappa \mu^\top x + \beta [(\gamma_1^\top x)^2 - (\gamma_2^\top x)^2]), \quad (5)$$

where β controls anisotropy and γ_1, γ_2 define principal axes.

Model selection via BIC. We evaluate model fit using the Bayesian Information Criterion (BIC):

$$\text{BIC} = -2 \log \mathcal{L} + k \log N, \quad (6)$$

Table 5: Directional distribution fitting across text encoders. Kent consistently achieves the lowest BIC and captures anisotropic structure, while vMF and moVMF remain isotropic ($\beta = 0$).

Encoder	\bar{r}	BIC (vMF)	BIC (moVMF)	BIC (Kent)	β/κ (Kent)
SD1.5 (CLIP-L)	0.88-0.96	-1.2e4	-1.3e4	-1.5e4	0.10-0.23
SDXL (OpenCLIP-G)	0.89-0.96	-2.0e4	-2.2e4	-3.1e4	0.13-0.25
SD3.5 (CLIP-G)	0.80-0.88	-8.1e3	-8.6e3	-9.9e3	0.10-0.14
SD3.5 (CLIP-L)	0.77-0.83	-4.2e3	-4.5e3	-5.3e3	0.08-0.13
FLUX (CLIP-L)	0.78-0.83	-4.3e3	-4.6e3	-5.4e3	0.08-0.13
T5-XXL	0.83-0.89	-2.8e4	-3.1e4	-3.2e4	0.03-0.14

where \mathcal{L} is the likelihood, k is the number of parameters, and N is the number of samples. Lower BIC indicates a better trade-off between fit quality and model complexity.

Results. Table 5 summarizes results across all concepts and encoders. Kent consistently achieves the lowest BIC across all concept-encoder pairs, with a 100% selection rate, meaning in all cases Kent was found to be the best representative for concept distributions. The average anisotropy ratio is $\beta/\kappa \approx 0.12$, indicating consistent but moderate deviation from isotropy.

These results show that concepts are best modeled as anisotropic directional distributions rather than single directions or isotropic clusters. This justifies our use of Kent-based representations for control operations.

B Geodesic Traversal

We perform semantic edits on the unit hypersphere $\mathbb{S}^{D-1} = \{x \in \mathbb{R}^D : \|x\|_2 = 1\}$, where semantic similarity is governed by angular distance rather than Euclidean magnitude. Given normalized embeddings $u, v \in \mathbb{S}^{D-1}$, their geodesic distance is $\theta(u, v) = \arccos(u^\top v)$. The shortest path between them is the great-circle geodesic:

$$\text{Geo}(u, v; \lambda) = \frac{\sin((1-\lambda)\theta)}{\sin\theta}u + \frac{\sin(\lambda\theta)}{\sin\theta}v, \quad \lambda \in [0, 1]. \quad (7)$$

This corresponds to spherical interpolation (slerp), which preserves the intrinsic geometry of the embedding manifold.

To perform local edits, we additionally use logarithmic and exponential maps between the hypersphere and its tangent space. The logarithmic map projects a point $v \in \mathbb{S}^{D-1}$ onto the tangent space at u :

$$\text{Log}_u(v) = \frac{\theta}{\sin\theta}(v - \cos\theta u), \quad \theta = \arccos(u^\top v),$$

producing a tangent vector pointing from u toward v . Conversely, the exponential map lifts a tangent vector $\xi \in T_u\mathbb{S}^{D-1}$ back onto the hypersphere:

$$\text{Exp}_u(\xi) = \cos(\|\xi\|_2)u + \sin(\|\xi\|_2)\frac{\xi}{\|\xi\|_2}.$$

A geodesic step along tangent direction d with strength λ is thus $\text{Exp}_u(\lambda d) = \cos(\lambda)u + \sin(\lambda)d$.

HEART-S uses the geodesic operator to rotate a concept-aligned component from source anchor μ_s toward target anchor μ_t : $\mu_{s \rightarrow t} = \text{Geo}(\mu_s, \mu_t; \lambda)$. HEART-A instead computes an attribute direction in the tangent space and applies an exponential-map update from the current token embedding: $\hat{h}^{(p)} = \text{Exp}_{\hat{h}^{(p)}}(\lambda d_a)$.

C Experimental Setup

C.1 Setup Details

Evaluation Metrics We evaluate subject replacement using four metrics: (1) target-subject classification accuracy (**Acc**), computed using zero-shot CLIP classification between source and target concepts; (2) image-text alignment (**CLIP-T**), measured as cosine similarity between CLIP image

Table 6: Prompt pairs used for subject replacement evaluation.

Edit Type	Source Prompt	Edited Prompt
Car → Truck	“A car on a road”	“A truck on a road”
Dog → Wolf	“A dog in a forest”	“A wolf in a forest”
Cat → Dog	“A photo of a cat sitting on a chair”	“A photo of a dog sitting on a chair”
Apple → Orange	“An apple on a branch”	“An orange on a branch”
Horse → Zebra	“A horse running in a field”	“A zebra running in a field”
Bird → Eagle	“A bird flying over mountains”	“An eagle flying over mountains”
Boat → Ship	“A boat floating on the ocean”	“A ship floating on the ocean”
Bicycle → Motorcycle	“A bicycle parked beside a building”	“A motorcycle parked beside a building”

and text embeddings; (3) perceptual similarity (**LPIPS**) (Zhang et al. [2018]) For methods without segmentation masks, LPIPS and structural metrics are computed over the full image. Following the evaluation protocol of Text Sliders (Chiu et al. [2026]), we generate 500 image pairs per attribute using the base prompt “*image of a person, photorealistic*” across seeds 0 . . . 499. We evaluate four attributes: *age*, *smile*, *curly hair*, and *chubby*. Attribute strength is measured using Δ CLIP, computed between edited images and attribute-specific text prompts, while structural preservation is measured using LPIPS between original and edited images.

Baselines For subject replacement, we compare against: SEGA Brack et al. [2023], LEDITS++ Brack et al. [2024], and Direct Swap, which regenerates images directly from the edited prompt without preservation constraints. We additionally evaluate **HEART-inv**, which combines HEART traversal with DDIM inversion.

For attribute control, we compare against: Concept Sliders Gandikota et al. [2024], Attribute Control Baumann et al. [2025], and Text Sliders Chiu et al. [2026].

Implementation Details All experiments are performed on NVIDIA H200 GPUs and A100 GPUs. Subject replacement experiments are conducted on SD 1.5 and SDXL using ten base prompts, three prompt templates and five random seeds per concept pair. For HEART-S, geodesic traversal is performed in normalized text embedding space using edit strengths $\lambda \in [-1, 1]$ and prompt-dependent edit-start schedules (10% of denoising steps).

For HEART-A, we use SDXL as the primary evaluation backbone. All images are generated using 30 diffusion steps at resolution 512×512 . Attribute traversal is performed using geodesic updates in tangent space, with separate controls for CLIP-L and OpenCLIP-G embeddings. We use the best-performing configuration: geodesic mode, `edit_start_step=2`, and edit strengths selected from uniformly sampled traversal ranges.

Time taken for generating the images in inference-time edit while determining the concept anchor for pool is roughly 37s for 5 images, wherein the images are a part of control of one concept.

C.2 License Information

We will make our code publicly available on acceptance. We use the following models in our work:

- SD 1.5: <https://huggingface.co/stable-diffusion-v1-5/stable-diffusion-v1-5>
- SDXL: <https://huggingface.co/stabilityai/stable-diffusion-xl-base-1.0>
- SD3.5-medium: <https://huggingface.co/stabilityai/stable-diffusion-3.5-medium>
- Flux-Schnell: <https://huggingface.co/black-forest-labs/FLUX.1-schnell>

C.3 Prompts used for Subject Control

For subject replacement, we follow a prompt-pair evaluation protocol where a source subject token is replaced with a target subject token while preserving the remaining scene description. We evaluate both object-centric and animal-centric subject transitions across multiple environments and contextual layouts.

Table 7: Prompt pairs used for attribute control evaluation.

Attribute	Negative / Source Prompt	Positive / Target Prompt
Age	“A young person, photorealistic”	“An old person, photorealistic”
Smile	“A serious person, photorealistic”	“A smiling person, photorealistic”
Hair Texture	“A person with straight hair, photorealistic”	“A person with curly hair, photorealistic”
Body Shape	“A slim person, photorealistic”	“A chubby person, photorealistic”
Beard	“A clean-shaven man, photorealistic”	“A bearded man, photorealistic”
Glasses	“A person without glasses, photorealistic”	“A person wearing glasses, photorealistic”
Hair Color	“A person with black hair, photorealistic”	“A person with blonde hair, photorealistic”
Expression	“A calm person, photorealistic”	“An angry person, photorealistic”

C.4 Prompts used for Attribute Control

For attribute control, we follow a paired semantic-direction protocol similar to prior text-based editing works (Chiu et al. [2026]). Each attribute is represented using positive and negative prompt pairs that define the source and target semantic anchors used for geodesic traversal. For each attribute, we can have multiple such prompt pairs.

D Limitations of our work

HEART operates purely in text embedding space and does not directly manipulate cross-attention maps, latent trajectories, or diffusion features. As a result, extremely fine-grained spatial edits or precise object-localized modifications can remain challenging, particularly in highly compositional scenes with strong semantic overlap between subjects. Similarly, while our inversion-free formulation enables efficient and general editing, inversion-based pipelines can provide stronger reconstruction fidelity for certain real-image editing tasks. Also, models like FLUX-Schnell which have very few denoising steps might not be able to showcase a lot of control ability. Our method depends upon the denoising steps to be at least more than 5.

E SD3.5-medium and FLUX results

We observe consistent semantic control on SD 3.5-Medium across diverse subject replacement tasks, demonstrating that HEART generalizes effectively to modern multi-encoder diffusion architectures in Figure 9. On FLUX-Schnell, semantic edits remain observable, particularly for large object-level transitions such as car→truck. However, because FLUX-Schnell operates with an extremely short denoising trajectory (only 4 diffusion steps), the influence of text-space geometric traversal is comparatively limited. As a result, subtle or fine-grained subject changes, such as cat→dog, may not fully propagate through the denoising process, leading to weaker visible semantic transitions. Nevertheless, the results indicate that directional geometric control persists even under highly compressed diffusion schedules.

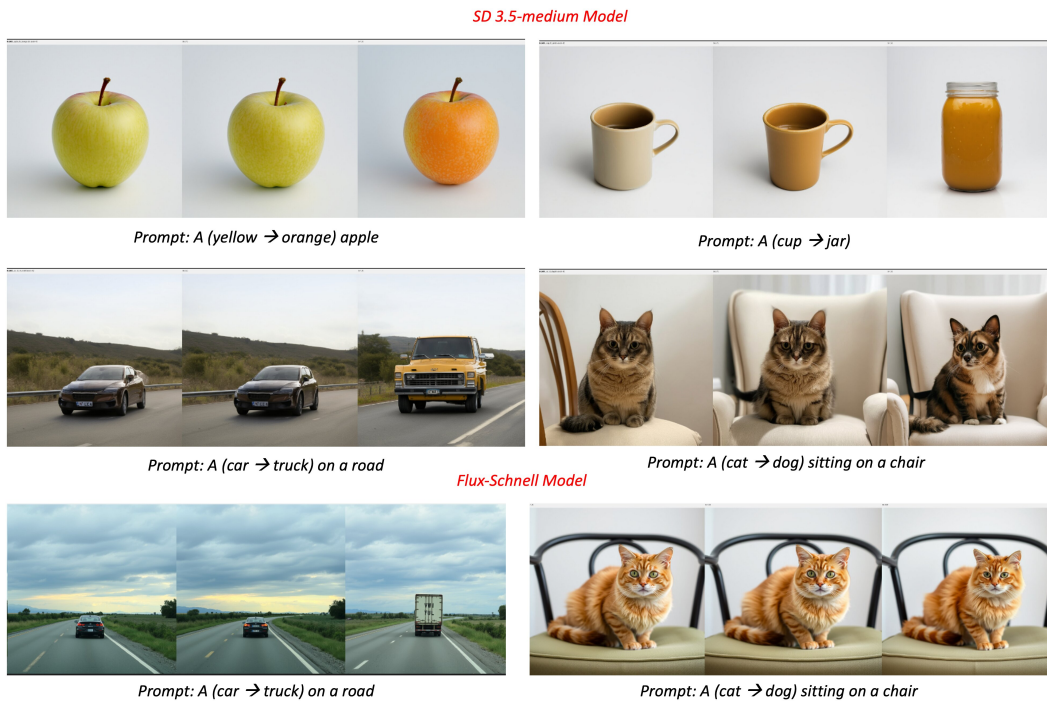


Figure 9: Cross-architecture subject control using HEART. Qualitative subject replacement results on SD 3.5-Medium (top two rows) and FLUX-Schnell (bottom row). HEART performs semantic traversal directly in text embedding space and generalizes across both CLIP- and T5-conditioned diffusion architectures. Despite large subject changes (e.g., apple→orange, car→truck, and cat→dog), the method preserves scene layout, viewpoint, lighting, and contextual structure while modifying only the target concept.